Short-range screening potentials for classical Coulomb fluids: Monte Carlo sampling and cluster model studies

Setsuo Ichimaru, Shuji Ogata, and Kenji Tsuruta
Department of Physics, University of Tokyo, Bunkyo, Tokyo 113, Japan
(Received 10 March 1994)

Screening potential, the balance between the bare Coulomb repulsion and the potential of mean force in a charged liquid, plays an essential role in the theoretical estimation of enhancement for the nuclear reaction rates in dense stellar matter. For the accurate assessment of the screening potential at short interparticle separations, we revisit the first-principles calculations for the coefficients of the Widom expansion and undertake extra-long Monte Carlo samplings in specifically designed binary-ionic systems. The results are compared with those obtained from an approximate estimation based on extrapolation from intermediate distances. We also present model calculations of the screening potential with two-ion clusters, which shed light on the relation between the short- and intermediate-range behaviors.

PACS number(s): 52.25.−b, 05.20.Gg

I. INTRODUCTION

The interparticle correlations and thermodynamic properties for various realizations of dense plasmas [1] have been investigated by computer simulation methods and by analytic means. In the simulation approach, the radial distribution functions for such plasmas have been sampled successfully by the Monte Carlo (MC) method [2–5] with the Metropolis algorithm [6].

Screening potential [7] is the balance between the bare Coulomb repulsion and the potential of mean force in such a charged liquid. Screening potentials at short interparticle distances play an essential role in the theoretical estimation of enhancement for the nuclear reaction rates in dense stellar matter [8]. The short-range correlations, which are not directly accessible in such a sampling of the radial distribution functions, have been approached through the first-principles analyses combining between the short-range Widom [9] expansion of the screening potential and direct MC samplings of the potential-field distributions at properly constructed test charges [10].

In the statistical theory of classical ensembles [11], it has been shown that the screening potential is intimately related to the increments of free energies between two realizations of many particle systems—a one-component plasma (OCP) and a corresponding binary-ionic mixture (BIM) plasma—before and after the nuclear reactions [8,12]. The seminal calculations for the enhancement factor for the thermonuclear reactions by Salpeter and Van Horn [13] were based on such a concept, where the free-energy increments were evaluated in terms of the ion-sphere model of Salpeter [14]. As improved construction of ion clusters over those of the ion-sphere model may shed new light on the nature of the screening potentials.

Separately, the short-range screening potentials were approached by a method of extrapolation [15–17] from the domain of intermediate distances where reliable information was available for the radial distribution functions. These may be termed as indirect methods, since the quantities defined in short ranges are inferred from intermediate distances comparable to the average interparticle spacings. No unambiguous predictions can be expected in such a scheme, however, since the results depend on the assumptions that one adopts for the extrapolation.

In this paper, we reexamine the first-principles calculation for the coefficients of the Widom expansion and perform extra-long MC samplings in the specifically designed binary-ionic systems [1,10]. We thereby evaluate the coefficients in significantly improved statistical accuracy, with the results which should settle an issue raised from the point of view of an approach based on extrapolation calculations [17,18]. We then present model calculations of the screening potential with improved constructions of two-ion clusters. The results, albeit approximate, corroborate the findings in the MC sampling calculations and shed light on the relation between short- and intermediate-range screening potentials.

II. SHORT-RANGE SCREENING POTENTIAL

A. Radial distribution function

We consider a classical OCP [8] consisting of N identical particles of electric charge Ze in a volume V with a uniform compensating charge background; $n=N/V$ is the average number density. The physical nature of such a plasma is characterized by a single dimensionless parameter,

$$\Gamma=\frac{\beta(Ze)^2}{a}\ , \tag{1}$$

called the *plasma parameter,* which measures the ratio between the average Coulomb energy and the average kinetic energy; β denotes the inverse temperature in energy units, and

$$a\equiv\left[\frac{3}{4\pi n}\right]^{1/3} \tag{2}$$

refers to the ion-sphere radius.

In a classical plasma, the joint distribution function between two particles separated at a distance r_{12}—that is, the *radial distribution function* $g(r_{12})$—is defined and calculated as

$$g(r_{12})=\left[1-\frac{1}{N}\right]\frac{V^2}{Q_N}\int d\mathbf{r}_3\cdots d\mathbf{r}_N \exp(-\beta\mathcal{H}_{\rm int}) . \tag{3}$$

Here the potential energy for a system consisting of N charged particles with relative spacings $r_{ij}=|\mathbf{r}_i-\mathbf{r}_j|$ and the neutralizing background (with the charge density $-\rho_e$) is given by

$$\begin{aligned}\mathcal{H}_{\rm int}&=\sum_{1\le i<j\le N}\frac{(Ze)^2}{r_{ij}}-\rho_e\sum_{1\le i\le N}\int d\mathbf{r}\frac{Ze}{|\mathbf{r}_i-\mathbf{r}|}\\&\quad+\tfrac{1}{2}\int d\mathbf{r}\,d\mathbf{r}'\frac{\rho_e^2}{|\mathbf{r}-\mathbf{r}'|}\\&=\sum_{2\le i\le N}\frac{(Ze)^2}{r_{1i}}+W_{N-1}(\mathbf{r}_2,\ldots,\mathbf{r}_N) .\end{aligned} \tag{4}$$

In Eq. (3),

$$Q_N=\int d\mathbf{r}_1 d\mathbf{r}_2\cdots d\mathbf{r}_N \exp(-\beta\mathcal{H}_{\rm int}) \tag{5}$$

is the *configuration integral* for the N-particle system, and the function W_{N-1} in Eq. (4) singles out the sum of all interactions except the ones involving the particle 1. The radial distribution functions are the probability densities of finding another particle 2 at a distance r_{12} away from a given particle 1, and are normalized so that they approach unity as the interparticle separations tend to infinity; particles separated at extremely large distances are not correlated with each other.

B. The Widom expansion of the screening potential

The *screening potential* is defined as

$$H(r)=\frac{(Ze)^2}{r}+\frac{1}{\beta}\ln[g(r)] . \tag{6}$$

It is the difference between the bare potential, the first term on the right-hand side, and the *potential of mean force* represented by the second term. The latter potential stems from a sum of a certain class of Mayer diagrams in the statistical-mechanical theory of liquids [11] and does not mean a real potential in the sense of particle dynamics. The screening potential is related closely to the bridge function in the theory of liquids [11,19], and plays an essential part in the theoretical treatment of an enhancement factor for the nuclear reaction rate due to many-body correlation [8].

It is instructive to investigate the short-range behavior of the screening potentials by expanding Eq. (6) in a power series of r^2 as

$$\beta H(r)=\beta H(0)+h_1(r/a)^2+h_2(r/a)^4+\cdots . \tag{7}$$

When calculating the coefficients in this expression, we find it instructive to rewrite Eq. (3) as

$$\begin{aligned}&\exp\left[\frac{\beta(Ze)^2}{r}\right]g(r)\\&=\frac{\langle\exp(-2\beta\psi)\rangle}{\langle\exp(-\beta\psi)\rangle^2}\\&\quad\times\frac{\langle\exp[-\beta\psi(\mathbf{r}')]\exp[-\beta\psi(\mathbf{r}'+\mathbf{r})]\rangle}{\langle\exp(-2\beta\psi)\rangle} .\end{aligned} \tag{8}$$

Here

$$\psi(\mathbf{r}_1)\equiv\sum_{2\le i\le N}\frac{(Ze)^2}{r_{1i}} \tag{9}$$

and the statistical average $\langle\ \rangle$ in Eq. (8) is defined and calculated as

$$\begin{aligned}&\langle f(\mathbf{r}_1-\mathbf{r}_2)\rangle\\&\equiv\frac{\int d\mathbf{r}_1 d\mathbf{r}_2\cdots d\mathbf{r}_N f(\mathbf{r}_1-\mathbf{r}_2)\exp(-\beta W_{N-1})}{\int d\mathbf{r}_1 d\mathbf{r}_2\cdots d\mathbf{r}_N\exp(-\beta W_{N-1})} .\end{aligned} \tag{10}$$

The value of the screening potential at $r=0$ may be evaluated by noting that the excess part $F_{\rm ex}$ of the Helmholtz free energy—that is, the interaction free energy—for the N-particle system is given in terms of the configuration integral (5) as

$$F_{\rm ex}=-\frac{1}{\beta}\ln\left[\frac{Q_N}{V^N}\right] . \tag{11}$$

For an OCP, one thus derives a relation [12],

$$\begin{aligned}H(0)&=\frac{1}{\beta}\ln\frac{\langle\exp(-2\beta\psi)\rangle}{\langle\exp(-\beta\psi)\rangle^2}\\&=F_{\rm ex}^{\rm BIM}(N,0)-F_{\rm ex}^{\rm BIM}(N-2,1) ,\end{aligned} \tag{12}$$

where $F_{\rm ex}^{\rm BIM}(N_1,N_2)$ denotes the excess free energy of a BIM plasma consisting of N_1 ions with charge number Z and N_2 ions with charge number $2Z$. Extension of Eq. (12) to a multi-ionic plasma is straightforward [5].

C. Coefficients of the expansion

We now perform a short-range expansion of Eq. (8) in a power series of r^2, which may be expressed as [9,12]

$$\begin{aligned}&\exp\left[\frac{\beta(Ze)^2}{r}-\beta H(0)\right]g(r)\\&\quad=\sum_{\nu=0}^{\infty}\frac{(-1)^\nu r^{2\nu}}{(2\nu)!}\left\langle\left[e^{\beta\psi}\frac{\partial^\nu}{\partial z^\nu}e^{-\beta\psi}\right]^2\right\rangle_{\rm BIM} .\end{aligned} \tag{13}$$

Here z represents one of the Cartesian components of $\mathbf{r}$ and the statistical average denoted by $\langle\ \rangle_{\rm BIM}$ is defined and calculated in accordance with

$$\begin{aligned}&\langle f(\mathbf{r}_1-\mathbf{r}_2)\rangle_{\rm BIM}\\&\equiv\frac{\int d\mathbf{r}_1 d\mathbf{r}_2\cdots d\mathbf{r}_N f(\mathbf{r}_1-\mathbf{r}_2)\exp(-\beta W_N')}{\int d\mathbf{r}_1 d\mathbf{r}_2\cdots d\mathbf{r}_N\exp(-\beta W_N')} ,\end{aligned} \tag{14}$$

where

$$W'_N \equiv 2\psi(\mathbf{r}_1) + W_{N-1} \tag{15}$$

refers to the potential energy of a BIM system in which one "test" particle has an electric charge $2Ze$ and each of the rest of $N-1$ particles has a charge Ze.

In light of Eq. (13), it is now straightforward to calculate the coefficients of the expansion (7); the results are [10]

$$\frac{h_1}{\Gamma} = -\frac{a^2\Gamma}{2}\left\langle \left[\frac{\partial}{\partial z}\left[\frac{\beta\psi}{\Gamma} \right] \right]^2 \right\rangle_{\mathrm{BIM}}, \tag{16}$$

$$\frac{h_2}{\Gamma} = \frac{a^4\Gamma^3}{24}\left\langle \left\{ \left[\frac{\partial}{\partial z}\left[\frac{\beta\psi}{\Gamma} \right] \right]^2 - \frac{1}{\Gamma}\left[\frac{\partial}{\partial z} \right]^2 \left[\frac{\beta\psi}{\Gamma} \right] \right\}^2 \right\rangle_{\mathrm{BIM}} - \frac{a^4\Gamma^3}{8}\left\langle \left[\frac{\partial}{\partial z}\left[\frac{\beta\psi}{\Gamma} \right] \right]^2 \right\rangle_{\mathrm{BIM}}^2 . \tag{17}$$

Since one calculates

$$\left\langle \left[\frac{\partial\psi}{\partial z} \right]^2 \right\rangle_{\mathrm{BIM}} = \frac{1}{6\beta}\Delta\psi = \frac{(Ze)^2}{2\beta a^3} \tag{18}$$

by partial integrations for a Coulombic system, Eq. (16) reduces to an identity [12]

$$\frac{h_1}{\Gamma} = -\frac{1}{4} . \tag{19}$$

Though the last term of Eq. (17) can be rewritten as $-\Gamma/32$ in light of the identity (18), we stress that h_2/Γ should be sampled *without* this replacement in Eq. (17) for securing statistical accuracy in the evaluation.

III. MONTE CARLO SIMULATION STUDIES

A. The coefficient h_2

Ogata, Iyetomi, and Ichimaru [10] undertook the direct MC sampling calculations of Eqs. (16) and (17) in a BIM system with N (=249) particles, of which 248 particles had a charge Ze and one with $2Ze$. Since the value of h_1/Γ is known by the identity (19), the direct calculation of Eq. (16) is useful in assessing the statistical accuracy of the MC sampling.

Let c denote the number of MC configurations generated in the Metropolis algorithm. These authors started with random initial configuration and waited for equilibration over the initial period of $c/N = 0 \rightarrow 6000$; the subsequent period, $c/N = 6000 \rightarrow 7000$, was then used for the direct calculations of the coefficients, $-4h_1/\Gamma$ and h_2/Γ, by the MC samplings of Eqs. (16) and (17). For comparison with the present calculations, we list the results obtained in those calculations by lightface numbers in the parentheses in Table I. These results are plotted also in Fig. 1.

On the basis of these data, it has been concluded [8,10] that

$$h_2/\Gamma = 0.00 \pm 0.01 . \tag{20}$$

TABLE I. The calculated values of the coefficients, $-4h_1/\Gamma$ and h_2/Γ, by the direct MC samplings of Eqs. (16) and (17). The boldface numbers are the results of the present calculations ($N=1000$); the lightface numbers in the parentheses are those of the earlier calculations ($N=249$) in Ref. [10].

Γ	$-4h_1/\Gamma$	h_2/Γ	Sampling (c/N)
160	**0.995**	**−0.0007±0.034**	**6000→68 000**
	(1.008)	(0.06±0.13)	(6000→7000)
80	**1.0018**	**0.021±0.022**	**6000→52 000**
	(0.991)	(−0.07±0.07)	(6000→7000)
40	**1.0009**	**0.011±0.015**	**6000→28 000**
	(0.992)	(−0.03±0.04)	(6000→7000)
10	**0.9996**	**0.004±0.012**	**6000→16 000**
	(0.989)	(0.0006±0.009)	(6000→7000)

Though the assessment (20) is consistent with all the data in that series of simulations, it was desired to perform direct MC sampling calculations with a significantly improved statistical accuracy, because of the relatively large error bars involved in those calculations especially at $\Gamma = 160$.

We have thus reexamined the MC sampling calculations of the coefficients, h_1 and h_2, in a *larger* system with N (=1000) particles, of which 999 particles have a charge Ze each and one with $2Ze$. The initial periods of $c/N = 0 \rightarrow 6000$ were again set aside for thermalization; the subsequent periods, listed in Table I, were then used for the direct calculations of the coefficients, $-4h_1/\Gamma$ and h_2/Γ, by the MC sampling. These samplings consumed a sum of 40 h in CPU time with the University of Tokyo HITAC S-3800/480 supercomputer. These results have been included in Table I by boldface characters and in Fig. 1 by the filled circles with thick error bars.

It is noteworthy that the statistical errors have now been reduced drastically and take on values close to the case with $\Gamma = 10$ in the 1991 simulations. In light of the values sampled for $-4h_1/\Gamma$, we might even conclude that the calculations are statistically as accurate as that case with $\Gamma = 10$. Obviously, the assessment (20) remains consistent with these improved data.

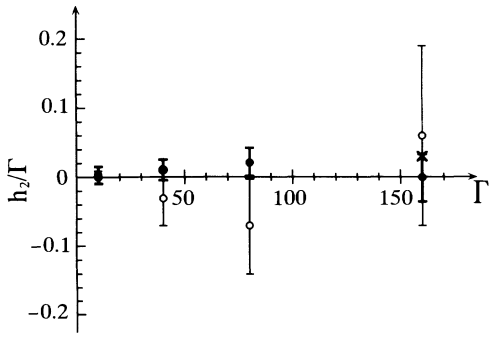

FIG. 1. The values of the coefficient $-h_2/\Gamma$ calculated by the MC samplings. The open circles with error bars represent the results of the earlier calculations in Ref. [10]; the filled circles with thick error bars, the present results; the ×, the evaluation by Rosenfeld in Ref. [17].

To examine the origin of improvement in the statistical accuracy achieved in the present simulation, we plot in Figs. 2 and 3 the values of $[-4h_1/\Gamma]_{2000}$ and $[h_2/\Gamma]_{2000}$ in the present sampling at $\Gamma=160$ as functions of c/N. Here $[\cdots]_{2000}$ denotes a statistical average in the sense of Eq. (16) or (17), however, over MC sampled data collected in a short interval of $\Delta c/N=2000$. We observe in these figures that each of the averages, $[-4h_1/\Gamma]_{2000}$ or $[h_2/\Gamma]_{2000}$, fluctuates enormously around unity or zero, respectively, and that their fluctuations are in phase more or less to each other; the use of Eq. (17) thus leads to partial cancellation between large fluctuations stemming from the first and second terms. Origin of the large departure from zero in the 1991 calculation of h_2/Γ at $\Gamma=160$ may be attributed to such a short interval ($\Delta c/N=1000$) of the sampling. To reduce the extents of errors involved in the statistical evaluation of h_1 and h_2, it is therefore necessary to perform very extended MC saplings as we have done in the present case. Establishing an effective measure in reducing the statistical errors in sampling of Eq. (16) leading to the identity, $h_1/\Gamma=-\frac{1}{4}$, likewise turns out essential for securing the accuracy in the sampling for h_2, since the former quantity enters the expression for the latter through the last term in Eq. (17).

B. The screening potential at zero separation

Values of the screening potential at zero interparticle separation, $H(0)$, may be obtained from balances of the BIM excess free energies in accordance with Eq. (12). The thermodynamic functions for dense BIM fluids have been investigated extensively for the construction of phase-separation diagrams associated with possible freezing transitions in the interiors of white dwarfs [20–22]. Substantial progress has been achieved due primarily to progress in the MC simulation studies [5].

We consider a BIM fluid in a volume V containing N_1 and N_2 particles of species "1" and "2" with charge numbers Z_1 and Z_2 ($>Z_1$), and number densities $n_1=N_1/V$ and $n_2=N_2/V$, respectively. The molar fraction of "i" species is denoted by $x_i=N_i/N$, where $N=N_1+N_2$;

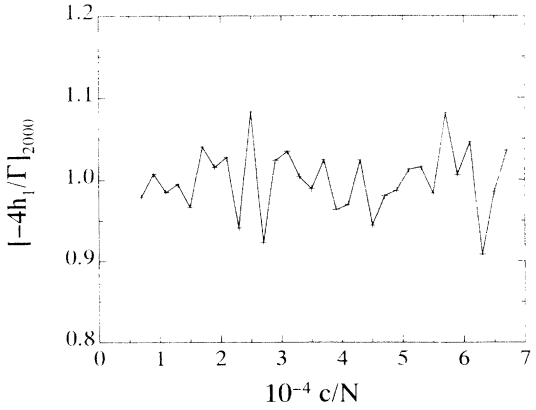

FIG. 2. Sequential evolution of the partial averages $[-4h_1/\Gamma]_{2000}$ in the present MC simulation at $\Gamma=160$. The solid lines are drawn only to guide the eye.

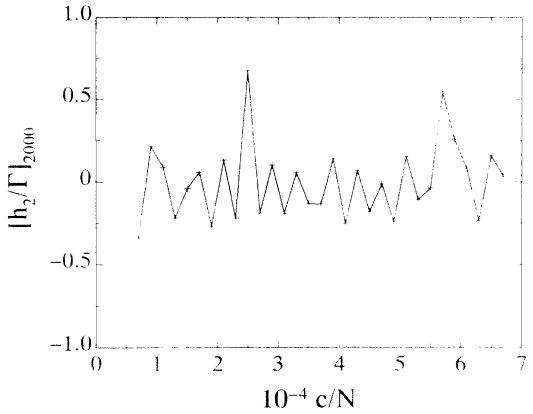

FIG. 3. Same as Fig. 2, but for the partial averages $[h_2/\Gamma]_{2000}$.

$R_Z=Z_2/Z_1$ denotes the charge ratio. The ion-sphere radius and the Coulomb coupling parameter of the individual species are defined as

$$a_i=\left|\frac{3Z_i}{4\pi n_e}\right|^{1/3}, \tag{21}$$

$$\Gamma_i=(Z_ie)^2\beta/a_i, \tag{22}$$

where n_e refers to the number density of the background electrons.

The excess internal energy of the BIM in units of N/β is calculated in terms of the partial radial distribution functions as

$$u_{\rm ex}^{\rm BIM}(R_Z,x,\Gamma_1)\equiv\sum_{i,j=1}^{2}\frac{\beta N x_i x_j}{2V}\int d\mathbf{r}\frac{Z_iZ_je^2}{r}[g_{ij}(r)-1]. \tag{23}$$

Here and hereafter in this section, we write $x=x_2$ for simplicity.

An extensive MC simulation study [5] of the excess internal energy (23) for BIM fluids has been performed at 37 different combinations of the parameter values $R_Z=\{4/3,3,5\}$, $x=0.01-0.5$, and $\Gamma_1=5-200$. In addition the present MC study contributes values of the BIM excess internal energy at $R_Z=2$ and $x=0.001$ for the four cases with different values of Γ_1, as listed in Table II. The results are compared with predictions from a *linear-mixing law*; that is,

$$u_{\rm ex}^{\rm LM}(R_Z,x,\Gamma_1)\equiv\sum_{i=1}^{2}x_iu_{\rm ex}^{\rm OCP}(\Gamma_i), \tag{24}$$

where

$$u_{\rm ex}^{\rm OCP}(\Gamma)=-0.898004\Gamma+0.96786\Gamma^{1/4}+0.220703\Gamma^{-1/4}-0.86097 \tag{25}$$

is the OCP excess internal energy in strong coupling [4,23]. With inclusion of the present cases of sampling for BIM, the MC results for the deviations,

$$\Delta u_{\rm ex}^{\rm BIM}=u_{\rm ex}^{\rm BIM}-u_{\rm ex}^{\rm LM}\ , \tag{26}$$

from the linear-mixing values are thus expressed in a different parametrized form as

$$\Delta u_{\rm ex}^{\rm BIM}(R_Z,x,\Gamma_1)=0.32\frac{\sqrt{R_Z-1}(xR_Z-0.11)}{R_Z-0.22}\times\exp(10.1-10.4x^{0.16})\times\frac{\Gamma_1 x(1-x)}{[\Gamma_1+100\exp(-5000x)]^2}\ . \tag{27}$$

This fit reproduces the previous MC data [5] for $0.01\le x\le 0.5$ as accurately as in Fig. 2 of Ref. [5]. Comparison of Eq. (27) with the present MC data at $x=0.001$ is given in Table II [24].

The excess Helmholtz free energy for a BIM fluid (in units of N/β) is expressed as a sum of the linear mixing contributions and the deviations therefrom:

$$f_{\rm ex}^{\rm BIM}=(1-x)f_{\rm ex}^{\rm OCP}(\Gamma_1)+xf_{\rm ex}^{\rm OCP}(\Gamma_2)+\Delta f_{\rm id}^{\rm BIM}(R_Z,x)+\Delta f_{\rm ex}^{\rm BIM}(R_Z,x,\Gamma_1)\ . \tag{28}$$

Here

$$f_{\rm ex}^{\rm OCP}(\Gamma)=-0.898004\Gamma+3.87144\Gamma^{1/4}-0.882812\Gamma^{-1/4}-0.86097\ln\Gamma-2.52692 \tag{29}$$

is the free energy for the OCP fluids assuming $f_{\rm ex}^{\rm OCP}(\Gamma=1)=-0.4363$ [4],

$$\Delta f_{\rm id}^{\rm BIM}(R_Z,x)=\sum_{i=1}^{2}x_i\ln\left[\frac{n_iZ_i}{n_e}\right]=(1-x)\ln\left[\frac{1-x}{1-x+xR_Z}\right]+x\ln\left[\frac{xR_Z}{1-x+xR_Z}\right] \tag{30}$$

refers to a free-energy contribution of the ideal-gas entropy of mixing under the condition of charge neutrality at a constant density of the background electrons. The last excess part in Eq. (28) can be evaluated from Eq. (27) via the technique of the coupling-constant integrations [1,5] as

$$\Delta f_{\rm ex}^{\rm BIM}(R_Z,x,\Gamma_1)=0.32\frac{\sqrt{R_Z-1}(xR_Z-0.11)}{R_Z-0.22}\exp(10.1-10.4x^{0.16})\times x(1-x)\left[\frac{1}{1+100\exp(-5000x)}-\frac{1}{\Gamma_1+100\exp(-5000x)}\right]+0.0551\frac{(R_Z-1)^{1.8}x(1-x)}{1+1.12(R_Z-1)x}\ . \tag{31}$$

As we have remarked [5], the deviations (31) in the BIM thermodynamic functions from the linear mixing evaluations are significant.

The screening potential at zero interparticle separation, Eq. (12), is thus evaluated as [8]

$$\beta H(0)=2f_{\rm ex}^{\rm OCP}(\Gamma)-f_{\rm ex}^{\rm OCP}(2^{5/3}\Gamma)-\frac{\partial}{\partial x}\Delta f_{\rm ex}^{\rm BIM}(2,x,\Gamma)\bigg|_{x=0}\ . \tag{32}$$

In Table III, we compare these evaluations with the values set forth in Ref. [10],

$$\beta H(0)_{\rm OII}=\Gamma(1.356-0.0213\ln\Gamma)-\Gamma(0.456-0.0130\ln\Gamma)^2\ , \tag{33}$$

and with those in a linear-mixing approximation,

$$\beta H(0)_{\rm LM}=2f_{\rm ex}^{\rm OCP}(\Gamma)-f_{\rm ex}^{\rm OCP}(2^{5/3}\Gamma)\ . \tag{34}$$

It is clear that the thermodynamic evaluations (32) agree closely with the OII evaluations (33). This points to the accuracy of Eq. (33) and importance of taking into account the deviations from linear mixing approximation

TABLE II. The BIM excess internal energies $u_{\rm ex}^{\rm BIM}$ sampled in the present simulation (cf. Table I) and departures $\Delta u_{\rm ex}^{\rm BIM}$ from the linear mixing values $u_{\rm ex}^{\rm LM}$ in Eq. (24).

Γ	$u_{\rm ex}^{\rm BIM}$	$\Delta u_{\rm ex}^{\rm BIM}$	Fit, Eq. (27)
10	−8.0169±0.0007	−0.0021±0.0007	−0.001 33
40	−34.336±0.0011	0.001±0.0011	−0.000 37
80	−69.886±0.0015	0.002±0.0015	−0.000 19
160	−141.349±0.0027	0.000±0.003	−0.000 09

TABLE III. Values of the screening potential at zero interparticle separation evaluated in various theoretical schemes. $\beta H(0)_{\rm OII}$ corresponds to Eq. (33); $\beta H(0)$, the thermodynamic evaluation (32); and $\beta H(0)_{\rm LM}$, the linear mixing approximation (34).

Γ	$\beta H(0)_{\rm OII}$	$\beta H(0)$	$\beta H(0)_{\rm LM}$
10	11.254	11.328	10.993
20	22.365	22.611	21.912
40	44.437	44.800	43.528
80	88.275	88.462	86.425
160	175.325	174.602	171.743

such as (34) in evaluating the short-range screening potentials through the thermodynamic relations.

IV. CLUSTER-MODEL CALCULATIONS

Calculations of the screening potential may be approached approximately through consideration of the electrostatic energies in Coulomb clusters [1,25,26]. Let an N-particle Coulomb cluster be constructed by N particles with electric charge Ze situated in a neutralizing background of uniform charge-density distribution, $-\rho_e$, with a volume Ω, which satisfies the relation,

$$\rho_e \Omega = NZe \ . \tag{35}$$

The electrostatic energy of such a cluster is then calculated as

$$E_N = \sum_{1\le i<j\le N} \frac{(Ze)^2}{r_{ij}} - \rho_e \sum_{1\le i\le N} \int_\Omega d\mathbf{r} \frac{Ze}{|\mathbf{r}_i-\mathbf{r}|} + \tfrac{1}{2}\int_\Omega d\mathbf{r}\, d\mathbf{r}' \frac{\rho_e^2}{|\mathbf{r}-\mathbf{r}'|} \ . \tag{36}$$

We then define a quasipotential, meaning a *trial* screening potential, by

$$H_t(r) = 2E_1 - E_2 + \frac{(Ze)^2}{r} \ , \tag{37}$$

where r denotes the distance between the two particles in the two-particle cluster.

In Salpeter's ion-sphere model [14], one calculates E_1 for a single particle located at the center of spherical charge distribution with the ion-sphere radius a in Eq. (2) and E_2 for a two-particle cluster with a radius $2^{1/3}a$, as depicted in Fig. 4(a). One thus finds [7]

$$\frac{H_{\rm IS}(r)}{(Ze)^2/a} = 1.057 - \tfrac{1}{4}x^2 \ , \tag{38}$$

where $x = r/a$. In this ion-sphere model, therefore, Eq. (19) is recovered and $h_2 = 0$.

For an arbitrary value of r ($\neq 0$), it has been shown [26] that a spherical two-particle cluster of Fig. 4(a) does not always correspond to a configuration with a minimum of the cluster energy E_2. Instead one may consider a spheroidal (SD) structure of Fig. 4(b) or a spherocylindrical (SC) structure of Fig. 4(c) for a two-particle cluster, in which at each value of r the energy E_2 is minimized with respect to the variational parameters, ζ and η, under the constraint of Eq. (35). Specifically we define

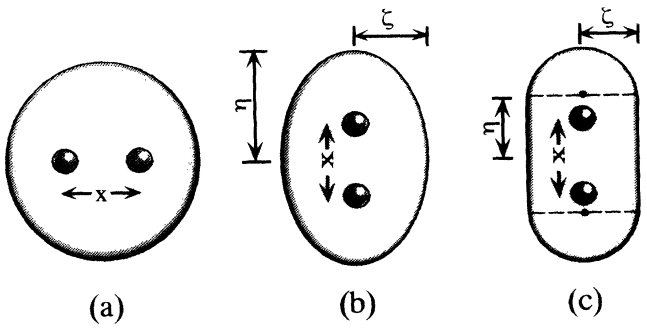

FIG. 4 Schematic views of two-particle Coulomb clusters with (a) spherical, (b) spheroidal, and (c) spherocylindrical structures.

a dimensionless screening potential in a cluster model as

$$h_c(x) \equiv \frac{H_t(r)}{(Ze)^2/a} = \frac{2E_1 - E_2}{(Ze)^2/a} + \frac{1}{x} \ , \tag{39}$$

which may be expressed for each of the elongated clusters as

$$h_c(x) = -1.8 - \frac{x^2}{4} - A[x;\zeta,\eta] + B[\zeta,\eta] \ . \tag{40}$$

Here, for a spheroidal cluster, we calculate

$$A[x;\zeta,\eta] = \frac{3}{8}\frac{1-\theta^2}{\theta^3}\left|\ln\left|\frac{1+\theta}{1-\theta}\right| - \frac{2\theta}{1-\theta^2}\right| x^2 \ , \tag{41}$$

$$B[\zeta,\eta] = \frac{3}{2^{1/3}}\frac{(1-\theta^2)^{1/3}}{\theta}\ln\left|\frac{1+\theta}{1-\theta}\right| - \frac{9}{32\pi^2}\int_\Omega d\mathbf{x}\, d\mathbf{x}' \frac{1}{|\mathbf{x}-\mathbf{x}'|} \ , \tag{42}$$

with

$$\theta = \left|1 - \left|\frac{\zeta}{\eta}\right|^2\right|^{1/2} \quad (\zeta < \eta) \ , \tag{43}$$

which has the meaning of a distortion parameter. The parameters, ζ and η, become functions of x, after the aforementioned variational calculations have been performed.

For a spherocylindrical cluster, we likewise calculate

$$A[x;\zeta,\eta] = -\frac{1}{2}\left|\frac{(\eta+x/2)^2-2\zeta^2}{\eta+x/2}\sqrt{(\eta+x/2)^2+\zeta^2} + \frac{(\eta-x/2)^2-2\zeta^2}{\eta-x/2}\sqrt{(\eta-x/2)^2+\zeta^2}\right| - \tfrac{3}{2}\zeta^2 \ln\left|\frac{\eta-x/2+\sqrt{(\eta-x/2)^2+\zeta^2}}{\eta+x/2-\sqrt{(\eta+x/2)^2+\zeta^2}}\right| - \frac{2\zeta^3\eta}{\eta^2-(x/2)^2} \ , \tag{44}$$

$$B[\zeta,n] = 3\zeta^2 - \eta^2 - \frac{9}{32\pi^2}\int_\Omega d\mathbf{x}\, d\mathbf{x}' \frac{1}{|\mathbf{x}-\mathbf{x}'|} \ . \tag{45}$$

In this case the deformation parameter is expressed as

$$\theta=\left[1-\left[\frac{\zeta}{\zeta+\eta}\right]^2\right]^{1/2} . \tag{46}$$

In Figs. 5 and 6, we plot the results of the variational calculations for θ and for $h_c(x)$ in the models of spheroidal and spherocylindrical clusters. In both cases, we observe $h_c(x)$ stay above the ion-sphere-model prediction (38), reflecting the fact that the elongated clusters do have the binding energies greater than the spherical ones. In the intermediate domain, $0.8\le x\le 1.8$, the calculated results may be fitted in linear forms,

$$h_c(x)=\begin{cases}1.25-0.398x & \text{(SD)}\\ 1.22-0.377x & \text{(SC)},\end{cases} \tag{47}$$

as exhibited in Figs. 5 and 6. Such a linear relation in the intermediate domain of the screening potential was first discovered by DeWitt, Graboske, and Cooper [15] through the analysis of MC data [2] for the OCP radial distribution functions.

For the analyses of the short-range behaviors of the screening potentials in the improved cluster-model calculations, we express

$$h_c(x)=h_c(0)+\xi_1 x^2+\xi_2 x^4+\cdots . \tag{48}$$

In both SD and SC cases, we find through direct calculations

$$\xi_1=\frac{1}{2!}\lim_{x\to 0}\frac{d^2}{dx^2}h_c(x)$$
$$=\frac{1}{2!}\lim_{x\to 0}\left[-\frac{1}{2}-\frac{\partial^2 A}{\partial x^2}\right]=-\frac{1}{4} \tag{49a}$$

and

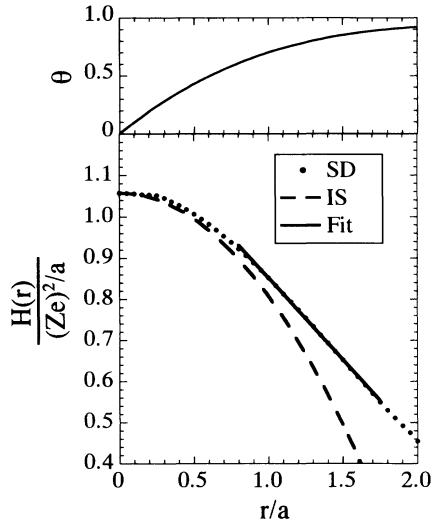

FIG. 5. Distortion parameter and screening potentials in the cluster-model calculations. The solid curve in the top and the dots in the bottom represent the results of the variational calculation for θ and $h_c(x)$, respectively, in the model of spheroidal (SD) cluster; the dashed curve, Salpeter's ion-sphere (IS) model; the solid line, the linear fit, Eq. (33), to the SD cluster values.

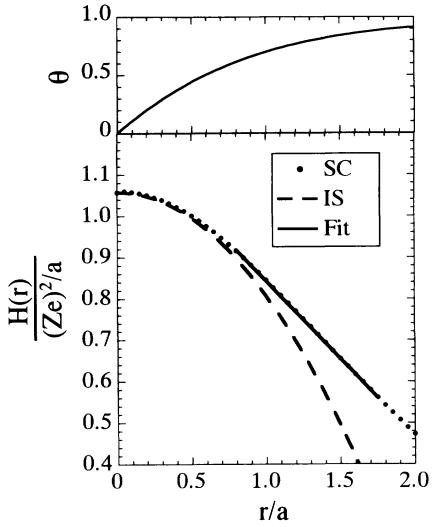

FIG. 6. Same as Fig. 5, but for θ and $h_c(x)$ in the model of spherocylindrical (SC) cluster.

$$\xi_2=\frac{1}{4!}\lim_{x\to 0}\frac{d^4}{dx^4}h_c(x)$$
$$=\frac{1}{4!}\lim_{x\to 0}\left[-\frac{\partial^4 A}{\partial x^4}-2\frac{\partial^2\theta}{\partial x^2}\frac{\partial^3 A}{\partial\theta\partial x^2}-\frac{\partial^3\theta}{\partial x^3}\frac{\partial^2 A}{\partial\theta\partial x}\right]=0 . \tag{49b}$$

The identity (19) is recovered in Eq. (49a), and the assessment (20) is again sustained in Eq. (49b). Mathematical proof of Eqs. (49) will be given in the Appendix.

It is instructive to compare implication of these model predictions, (47) and (49): Equation (47) implies that the screening potential is different in the intermediate domain between the SD and SC cases. The values of the short-range coefficients in Eqs. (49), on the other hand, are the same for both cases. This comparison therefore signals a warning against an uncritical use of an extrapolation method for estimation of the short-range quantities. We shall elaborate this point further in the next section.

V. METHODS OF EXTRAPOLATION

In 1973, DeWitt, Graboske, and Cooper [15] analyzed the MC data for $g(r)$ obtained by Brush, Sahlin, and Teller [2] and thereby found a linear relation for the screening potential, i.e., $h(x)=a_0-a_1x$, over an intermediate domain, $0.9<x<1.6$. This relation was then extrapolated toward the short range as

$$h(x)=1.205-\frac{0.1898}{\Gamma}-\frac{1}{2}x^2+\cdots .$$

In this work, the coefficient of the quadratic term is $-\frac{1}{2}$, which differs from that presented here in Eq. (19).

Subsequently in 1978, Alastuey and Jancovici [16] derived an overall approximate fit of $h(x)$ in the whole interval, $0\le x\le 1.6$, as

$$h(x)=h(0)-\tfrac{1}{4}x^2+0.039x^4-0.0043x^6 . \tag{50}$$

It must be noted that these authors have correctly termed this expression as "an overall approximate fit." The expression (50) has *not* been offered as a short-range expression in the sense of Eq. (7), though the coefficient of the quadratic term correctly reproduces the corresponding coefficient of expansion, $-\frac{1}{4}$, as in Eq. (19). It is therefore meaningless to compare the coefficient, 0.039, of the quartic term with an evaluation, such as Eq. (20), of the coefficient in the short-range expansion.

Finally in 1992, Rosenfeld [17] followed up the extrapolation method of DeWitt, Graboske, and Cooper [15], in which the MC data [10] of $g(x)$ in an intermediate domain have been used for an assessment of the coefficients of Widom expansion (7) in the short range; in particular, he obtained

$$h_2/\Gamma=0.03, \quad \text{at } \Gamma=160 . \tag{51}$$

This value is entered in Fig. 1 as well. Based on an extrapolation scheme, whose results depend on the adopted assumptions, the evaluation is an approximation. Though the estimated value (51) is still (barely) allowed by the error bars in the present direct calculation as listed in Table I, the observed trends in Fig. 1, coupled with our analytic model calculations, indicate that this estimate is unlikely to be supported in a first-principles evaluation based on Eq. (17) when the size of the MC sampling is further increased.

Rosenfeld recognized such an approximate nature on the extrapolation scheme and used the results mainly for justification of his another approximate "Onsager-molecule" concept. In his paper [17], Rosenfeld pointed out differences between the predicted values of $h(0)$ in his approach and those in Ogata, Iyetomi, and Ichimaru [10]. In Figs. 7 and 8, we compare the screening potentials obtained in the schemes of Ogata, Iyetomi, and Ichimaru [10] and of Rosenfeld [17] as well as those sampled by the MC simulation method; plotted therein also are the values of $h(0)$ computed by the thermodynamic

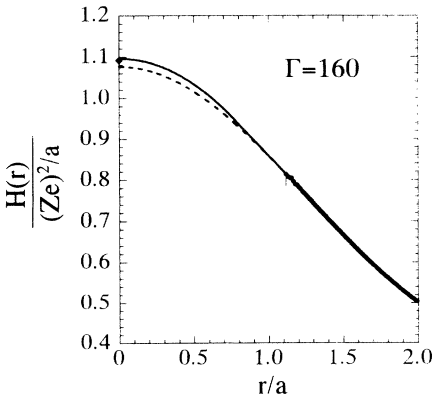

FIG. 7. Comparison of screening potentials for the OCP at $\Gamma=160$. The dots represent the MC data [10]; the maximum extent of statistical uncertainty in the MC sampling points is 10^{-5}, unless explicitly shown by vertical bars. The solid curve depicts the values of the fitting formulas obtained by Ogata, Iyetomi, and Ichimaru [10]; the dashed curve, by Rosenfeld [17]. The thermodynamic evaluation of $H(0)$, Eq. (32), is plotted by a filled diamond.

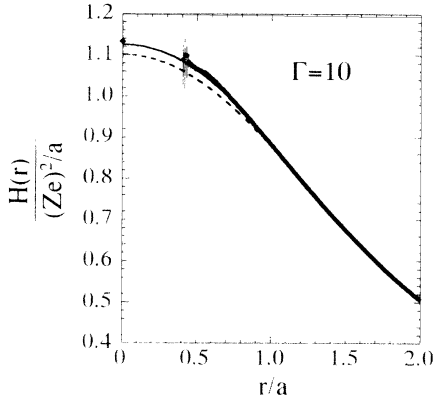

FIG. 8. Same as Fig. 7, but at $\Gamma=10$. The maximum extent of statistical uncertainty in the MC sampling points is 10^{-4}, unless explicitly shown by vertical bars.

evaluation, Eq. (32), where deviations from the linear-mixing law have been properly taken into account. The results of the present calculations and comparisons, shown in Tables I and III as well as in Figs. 1, 7, and 8, clearly indicate the accuracy of the first-principles schemes that have led to Eqs. (17), (20), (32), and (33) [27].

ACKNOWLEDGMENTS

The authors wish to thank Dr. H. E. DeWitt, Dr. H. Iyetomi, and Dr. H. M. Van Horn for their useful comments and discussions on these and related subjects. This research was supported in part by Grants-in-Aid for Scientific Research provided by the Ministry of Education, Science, and Culture of Japan through Research Grant Nos. 04455010 and 3005.

APPENDIX: PROOF OF EQS. (49)

In the cluster model actual shapes of the clusters are determined by the parameters, ζ, and η, which are related as

$$\eta=\begin{cases} 2/\zeta^2 & \text{for SD} \\ 2(2-\zeta^3)/(3\zeta^2) & \text{for SC,} \end{cases} \tag{A1}$$

through the condition of Eq. (35). The distortion parameters θ defined by Eqs. (43) and (46) is therefore the variational parameter, instead of ζ, to calculate the dimensionless screening potential in the model defined by Eq. (40) for a given x. The variational calculations are performed numerically so that

$$\left.\frac{\partial h_c}{\partial\theta}\right|_x=-\left.\frac{\partial}{\partial\theta}(A-B)\right|_x=0 , \tag{A2}$$

and the values of θ are obtained as a function of x (see Figs. 5 and 6).

To calculate the short-range expansion (48) of $h_c(x)$ with respect to x, we write the total derivatives of $h_c(x)$ in the second and fourth order as

$$\frac{d^2}{dx^2}h_c(x)=\frac{\partial^2 h_c}{\partial x^2}+\left[\frac{d\theta}{dx}\right]^2\frac{\partial^2 h_c}{\partial\theta^2}+2\frac{d\theta}{dx}\frac{\partial^2 h_c}{\partial\theta\partial x} \tag{A3}$$

and

$$\frac{d^4}{dx^4}h_c(x)=\frac{\partial^4 h_c}{\partial x^4}+\left[\frac{d\theta}{dx}\right]^4\frac{\partial^4 h_c}{\partial\theta^4}+4\left[\frac{d\theta}{dx}\right]^3\frac{\partial^4 h_c}{\partial\theta^3\partial x}+6\left[\frac{d\theta}{dx}\right]^2\frac{\partial^4 h_c}{\partial\theta^2\partial x^2}+\frac{d\theta}{dx}\left[4\frac{\partial^4 h_c}{\partial\theta\partial x^3}+2\frac{d^2\theta}{dx^2}\frac{\partial^3 h_c}{\partial\theta^2\partial x}+\frac{d^3\theta}{dx^3}\frac{\partial^2 h_c}{\partial\theta^2}\right]+2\frac{d^2\theta}{dx^2}\frac{\partial^3 h_c}{\partial\theta\partial x^2}+\frac{d^3\theta}{dx^3}\frac{\partial^2 h_c}{\partial\theta\partial x}\ , \tag{A4}$$

respectively. Figures 5 and 6 show that

$$\lim_{x\to 0}\theta(x)=0\ , \tag{A5}$$

and that

$$\lim_{x\to 0}\frac{d\theta}{dx}$$

takes on a finite value. Hence the second identities in Eqs. (49a) and (49b) are obtained by substituting Eq. (40) into Eqs. (A3) and (A4), respectively, with the condition (A2).

After straightforward calculations for both SD and SC cases, we find

$$\lim_{x\to 0}\frac{\partial^n h_c}{\partial x^n}=-\lim_{x\to 0}\frac{\partial^n A}{\partial x^n}=0\ , \tag{A6}$$

$$\lim_{x\to 0}\frac{\partial^2 A}{\partial\theta\partial x}=\lim_{x\to 0}\frac{\partial^3 A}{\partial\theta\partial x^2}=\lim_{x\to 0}\frac{\partial^3 A}{\partial\theta^2\partial x}=\lim_{x\to 0}\frac{\partial^4 A}{\partial\theta\partial x^3}=\lim_{x\to 0}\frac{\partial^4 A}{\partial\theta^3\partial x}=\lim_{x\to 0}\frac{\partial^4 A}{\partial\theta^2\partial x^2}=0\ , \tag{A7}$$

where $n=1$, 2, 3, and 4. Since we may assume that A, B, and their differentials are smooth and regular functions at $x=0$ and its vicinity, Eqs. (A6) and (A7) lead to the last identities in Eqs. (49a) and (49b).

[1] S. Ichimaru, *Statistical Plasma Physics Vol. II: Condensed Plasmas* (Addison-Wesley, Reading, MA, 1994).
[2] S. G. Brush, H. L. Sahlin, and E. Teller, J. Chem. Phys. **45**, 2102 (1966).
[3] J.-P. Hansen, Phys. Rev. A **8**, 3096 (1973).
[4] W. L. Slattery, G. D. Doolen, and H. E. DeWitt, Phys. Rev. A **21**, 2087 (1980); **26**, 2255 (1982).
[5] S. Ogata, H. Iyetomi, S. Ichimaru, and H. M. Van Horn, Phys. Rev. E **48**, 1344 (1993).
[6] N. Metropolis, A. W. Rosenbluth, M. N. Rosenbluth, A. H. Teller, and E. Teller, J. Chem. Phys. **21**, 1087 (1953).
[7] S. Ichimaru, Rev. Mod. Phys. **54**, 1017 (1982).
[8] S. Ichimaru, Rev. Mod. Phys. **65**, 255 (1993).
[9] B. Widom, J. Chem. Phys. **39**, 2808 (1963).
[10] S. Ogata, H. Iyetomi, and S. Ichimaru, Astrophys. J. **372**, 259 (1991).
[11] J.-P. Hansen and I. R. McDonald, *Theory of Simple Liquids*, 2nd ed. (Academic, London, 1986).
[12] B. Jancovici, J. Stat. Phys. **17**, 357 (1977).
[13] E. E. Salpeter and H. M. Van Horn, Astrophys. J. **155**, 183 (1969).
[14] E. E. Salpeter, Aust. J. Phys. **7**, 373 (1954).
[15] H. E. DeWitt, H. C. Graboske, and M. S. Cooper, Astrophys. J. **181**, 439 (1973).
[16] A. Alastuey and B. Jancovici, Astrophys. J. **226**, 1034 (1978).
[17] Y. Rosenfeld, Phys. Rev. A **46**, 1059 (1992).
[18] H. E. DeWitt, Contrib. Plasma Phys., Berlin **33**, 399 (1993).
[19] H. Iyetomi, S. Ogata, and S. Ichimaru, Phys. Rev. A **46**, 1051 (1992).
[20] D. Stevenson, J. Phys. (Paris) **41**, C2-61 (1980).
[21] J. L. Barrat, J.-P. Hansen, and R. Mochkovitch, Astron. Astrophys. **199**, L15 (1988).
[22] S. Ichimaru, H. Iyetomi, and S. Ogata, Astrophys. J. Lett. **334**, L17 (1988).
[23] S. Ogata and S. Ichimaru, Phys. Rev. A **36**, 5451 (1987).
[24] Since the value of $\Delta u_{\rm ex}^{\rm BIM}$, whose magnitude is already infinitesimally small at $x=0.001$, decreases with Γ_1 as $\sim 1/\Gamma_1$, comparison is meaningful only at $\Gamma_1=10$ in light of statistical accuracy.
[25] K. Tsuruta and S. Ichimaru, Phys. Rev. A **48**, 1339 (1993).
[26] K. Tsuruta, Ph.D. thesis, University of Tokyo, 1994.
[27] In Table II of Ref. [18], DeWitt analyzed the two cases of his own MC sampling data for the BIM excess internal energy, and concluded that "deviations from linear mixing are always positive." However, using his MC and LM values for the excess internal energy at $Z_2=5$, we find that this deviation takes on a *negative* value of -0.001, which is rather close to the value, -0.002 ± 0.001, obtained by Ogata, Iyetomi, and Ichimaru [10] for the same case.

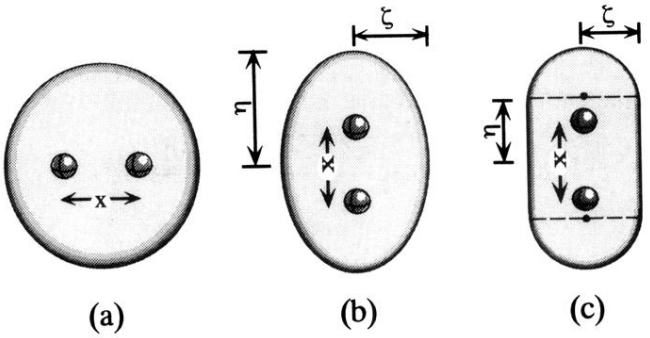

FIG. 4 Schematic views of two-particle Coulomb clusters with (a) spherical, (b) spheroidal, and (c) spherocylindrical structures.